Structural Design Using Principal Stress Line for Toolpath-based

Additive Manufacturing

Eder da Silva Sales

A Thesis

in

The Department

of

Mechanical, Industrial

and

Aerospace Engineering

Presented in Partial Fulfillment of the Requirements

for the Degree of Master of Applied Science at

Concordia University

Montreal, Quebec, Canada

September 2019

CONCORDIA UNIVERSITY

School of Graduate Studies

This is to certify that the thesis prepared

By: Eder da Silva Sales

Entitled: Structural Design Using Principal Stress Line for Toolpath-based

               Additive Manufacturing

and submitted in partial fulfillment of the requirements for the degree of

Master of Applied Science

complies with the regulations of the University and meets the accepted standards with

respect to originality and quality.

Signed by the final Examining Committee:

_____ Chair

Dr. Farjad Shadmehri

_____ Examiner

Dr. Ayhan Ince

_____ Examiner

Dr. Yong Zeng

_____ Supervisor

Dr. Tsz Ho Kwok

Approved by   _____

Chair of Department or Graduate Program Director

_____ _____

    Date   *Dean of Faculty*

CONCORDIA UNIVERSITY

Abstract

Structural Design Using Principal Stress Line for Toolpath-based

Additive Manufacturing

by Eder da Silva Sales

The use of additive manufacturing (AM) has increased considerably in recent years. This technology has been used in many areas due to the possibility of creating complex shapes in an easy, fast, and without wasting material. This creative freedom also allows components to be highly optimized according to their function. Currently, there are advanced algorithms that allow final users to perform topology optimization in the computer-aided design (CAD) phase. However, the optimization results might not be respected or considered during the downstream AM planning processes like slicing hence the optimized structural design may be lost during the actual fabrication process. This work has a focus on topology optimization during the toolpath planning process, instead of only in the CAD phase, by taking into account the toolpath characteristics presented in the AM processes. For an AM process whose toolpath is a set of lines such as fused deposition modeling (FDM), this thesis develops a line based topology optimization using the principal stress line (PSL) as the guidance in generating optimized toolpaths. The method is efficient, controllable, and able to consider the characteristics of the AM process. The computation results can be directly converted into toolpaths, so that the fabrication will follow faithfully as what is planned. Experimental structural tests were performed on the proposed method and the results obtained demonstrate that the strategy of applying PSL-based optimization in toolpath planning is a promising direction to complement the topologically optimized results from the CAD phase.

Acknowledgements

Contents

List of Figures

List of Tables

List of Abbreviations

PSL   Principal Stress Line

CAD   Computer-Aided Design

CAM   Computer-Aided Manufacturing

FEA   Finite Element Analysis

AM   Additive Manufacturing

SIMP   Solid Isotropic Material Penalization

TO   Topology Optimization

GS   Ground Structure

FDM   Fused Deposition Modeling

LS   Level Set

1 Introduction

In the toolpath-based additive manufacturing (AM) processes such as fused deposition modeling (FDM), a computer-aided design (CAD) model is first converted to a geometric file like a set of triangular meshes. The model is then processed by computer-aided manufacturing (CAM) software to generate motion control instructions that can be used by an AM printer [1]. Most AM processes nowadays accumulate material layer-by-layer. Thus, the CAM software needs to slice the three-dimensional (3D) geometry into multiple two-dimensional (2D) layers. Each layer can be formed by depositing material on layer boundary followed by constructing an internal structure known as the infill of the interior area. The infill is responsible to increase component strength and also works as a support structure for the upper layers. The infill can be defined as a percentage of the filled volume, in which 100% infill means that the component is fully filled. To reduce weight and fabrication time, different combinations of infill patterns and percentage can be selected [2, 3]. Research shows that appropriate construction of filling patterns can improve parts for their intended function as well as part quality and print efficiency [4, 5, 6, 7]. The AM technology can fabricate components with better quality for a wider range of applications if suitable infills for the 3D printed layers are used based on functional design requirements.

To utilize the capability of AM, several optimization tools have been developed for structures as well as the infill [8]. Modern CAD software can perform optimization on size, shape and topology [9, 10]. Size and shape optimization find the optimal size of elements and the location of nodes for a given structure, while topology optimization (TO) optimizes material distribution within a given domain. The inputs of the method are normally applied loads and boundary constraints. Using TO, optimized design can
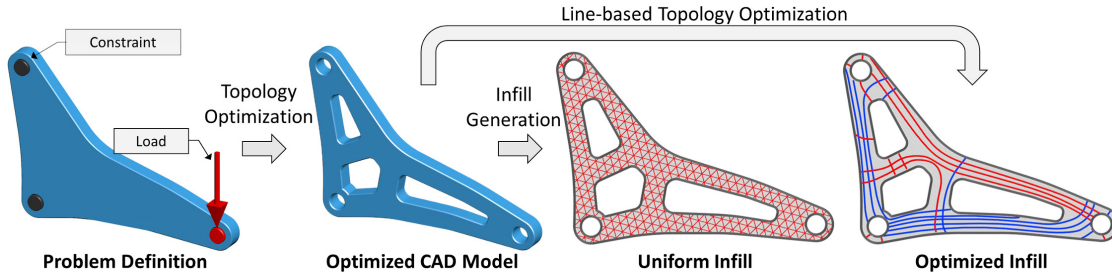
FIGURE 1.1: When topology optimization is only applied in the CAD model, the generated infill pattern during slicing may not reflect its structural properties. This work proposes a line-based topology optimization using principal stress line (PSL) to generate an optimized infill as well as the toolpaths for fabrication.

be generated for 3D-printed parts considering functionality besides the geometry it-self, e.g., maximizing stiffness. TO algorithms have been successfully implemented in modern CAD software. However, typical TO methods do not consider manufacturing parameters and produce an output with a limited resolution, which cannot be used for process planning directly. For example, while the high complex geometries obtained via TO can be fabricated by FDM, the final toolpath used to produce the part is determined by the slicer (illustrated in Fig. 1.1). As FDM 3D printing has anisotropic properties, if the toolpath does not follow the TO results, it could limit or even reduce the structural strength obtained during the CAD phase. For example, one of the worst cases is that the TO result from the CAD phase is in the vertical direction but the toolpaths generated by slicing are all in the horizontal direction.

This observation motivates this research to connect the TO results with the slicing operations, such that the fabrication obeys the design. The goal is to apply topology optimization in the toolpath planning to realize functional slicing for additive manu-facturing. Nevertheless, there are a few challenges prohibiting the realization of this objective. First, TO is usually a computationally expensive process (e.g., at least a few minutes), and if it is applied to each single layer in the slicing, that will be unrealistic for process planning. Second, the TO results are generally discretized (e.g., pixels), but the toolpaths are a set of lines, so the conversion between them is unclear. Furthermore, if a small-size domain is used to compromise on the speed, the TO results will be in

low-resolution and the generation of toolpath will be even more challenging. The contributions of this work come from overcoming these challenges. Inspired by a structural topology design method based on principal stress lines (PSL) [11], the objective is to develop a line-based topology optimization that can generate toolpaths efficiently and directly without the need of conversion from other representations to lines (the rightmost of Fig. 1.1). PSL is a line following the direction of principal stress where only the normal stresses exist, and the material located along the PSL will provide the maximum strength for the structure. To plan the toolpath using PSL, the manufacturing parameters must be considered, and the contributions are summarized as follows:

1. The PSL method is applied in toolpath planning that takes the stress field as input and outputs the topologically optimized toolpath in a few milliseconds.

2. A tensile and compression classification is done on the PSLs, so that the PSLs can be printed in proper order to support the loads considering the manufacturing method.

3. For the non-uniform infill pattern generated by PSLs, a binary search method is developed to find the optimal number of PSLs that can give the desired infill ratio.

4. The relationship between extrusion rate and line width is studied, and the extrusion rate is controlled to avoid material overlapping and properly respect the PSLs.

Experimental results show that this line-based topology optimization is promising for toolpath planning in terms of the efficiency and the printability. Physical tests demonstrate that the optimized toolpath can redistribute the stresses while uniform infills have the stresses concentrated in the same regions. A destructive test is also done and shows that there is a 50% improvement in mechanical strength with the same amount of material used.

The rest of this work is organized as follows. Related works are reviewed in Chapter 2. In Chapter 3, it is presented an overview of the method and the fundamentals. Chapter 4 presents the technical details in applying PSL with the consideration in manufacturing. It is followed by the experimental results in Chapter 5. This work is concluded in Chapter 6 with a discussion.

2 Related Work

This chapter is going to review works related to topology optimization and infill generation. Structural optimization is an important discipline, with great applicability in different areas of engineering [12, 13]. It is used, for example, to define the beam profile of a bridge, the best wing structure of an aircraft, or to find the best material distribution in a car dashboard. A classical optimization problem has an objective function $f(\mathbf{x})$ to be minimized. Examples of objective functions are stress, weight, cost, etc. This function is subjected to inequality and equality constraints, $g(\mathbf{x})$ and $h(\mathbf{x})$, where $\mathbf{x}$ is the vector of a design variables $\mathbf{x} = (x_1, x_2, ..., x_n)$ [14]. An example of design variable is the thickness of a plate or the diameter of a hole in a fuselage. The improvement of computational power allowed the use of finite element models to perform numerical optimization, being initially used to optimize the size of simple beams. Developments in this area started in the 1960s with the work of Schmit [15].

Recently, shape and topology optimization have been largely studied. Shape optimization considers, as design variables, control points in the domain borders. With the variation of the position of this points, the domain shape is modified [16]. Pironneau [17] demonstrate numerical techniques to perform shape optimization for elliptic systems, one example of an application for this method is the aerodynamic performance optimization of wings airfoils, as shown in [18, 19, 20]. These studies were able to obtain the optimal wing profile considering as objective drag minimization. Bendsøe and Kikuchi [21] introduces Topology Optimization. Differently from shape optimization, TO can remove material, adding holes, and changing the shape of the domain. The design variable is the density of each domain cell, varying from 0 to 1, where 0 is the absence of material.

To find the optimum solution, different methods are used. Gradient-based Methods as Quasi-Newton, Conjugate Gradient, Sequential Quadratic Programming (SQP) [22], are used to obtain the global optimum of the objective function. Heuristic Methods as Genetic Algorithms (GA) [23] and Simulated Anneling are also used. However, they are more used to find the local optimum.

2.1   Optimization strategies

During the component design in the CAD phase, topology optimization can be applied to reduce material usage while still satisfying the required objective function. Different TO methods are available [24], such as Level Set, Solid Isotropic Material Penalization (SIMP) and Ground Structure (GS).

The level set method was presented by Osher and Sethian [25]. It is able to follow the motion of a front whose speed depends on the local curvature with a Eulerian approach. The front is defined in an implicit way. In two dimensions, it represents a closed curve, where the level set function ϕ takes positives values in the region inside the curve and negatives values in the outside region. The level set equation is a partial differential equation and can be solved using numerical methods, such as finite-difference methods or Godunov's scheme [26]. It has been used in different research areas, such as image processing, fluid dynamics, structural optimization, etc.

In structural optimization, Sethian and Wiegmann [27] developed a method to solve Lamé equations, calculate the stress and optimize the design using level set to perturb the given shape and interact until an improved design is obtained. Allaire, Jouve, and Toader [28] were able to perform shape optimization combining level set with shape gradient. One advantage of this method is the moderate computational cost. In posterior work, the level set was combined with shape derivative [29] in two and three dimensions, considering linear and nonlinear elasticity. One disadvantage encountered in their method is the strong dependence between the optimal solution and the initial guess. Wang, Wang, and Guo [30] demonstrate the flexibility of level set methods to handle complex domain changes. Allaire and Jouve [31] coupled level set with a

topological derivative to develop an algorithm for TO. Suresh and Takalloozadeh [32] developed a stress-constrained TO. Xia et al. [33] use the level set to solve the shape and topology optimization problem minimizing the global measure of stress. A MATLAB code to run level set TO is available online [34].

SIMP is a popular TO strategy [35]. In this strategy, the design domain ω is discretized into finite elements. Isotropic material properties are assigned for each element. The design variable vector **x** contains the density of the elements. To obtain better topology intermediate densities are penalized using a factor p to control the lower stiffness values Finite element analysis gives the stiffness tensor E. The relationship between the element density and material is given by the power-law, $E(\mathbf{x}) = (\mathbf{x})^p E^0, p > 1$, where E^0 is the solid material stiffness tensor, and p is the penalty factor [36, 37]. The main function of p is to avoid fractional densities. SIMP is a computationally efficient, robust method able to adapt to different design conditions [38].

Despite the advantages, the method is mesh-dependent. Therefore, to produce high-resolution results a fine mesh must be created. As a consequence, the finite element analysis necessary to compute the stress tensors can become computationally expensive. It can also produce intermediate densities, being dependent on the degree of penalization [39]. Also, due to the nonconvex nature of penalized problems, there is a high possibility of local minima [40]. To avoid such behavior continuation methods have been proposed. It increases the chances to obtain global minima. In this method, the first interaction does not contain penalization. Therefore the problem becomes convex. After solving the convex problem, the penalization is added and the nonconvex problem using the results of first-run as the start point is solved. This step is repeated, increasing the penalization, and using the previous results as the start point to the new interaction. Examples of the method can be seen in [41, 42, 43].

Based on the SIMP method there is the Rational Approximation of Material Properties (RAMP) [44, 45], which introduces new penalization methods to allow convex functions for any penalization parameter. Another method based on SIMP is the Optimal Microstructure with Penalization (OMP) [46, 47], with a 1 and 0 penalization method.

However, this method is also nonconvex and requires more computational effort than SIMP.

Proposed by Dorn [48], the Ground Structure (GS) method is largely used in TO of trusses. Since GS algorithm only allows the removal of bars, a high-density initial structure is necessary to obtain good optimization results. To overcome this limitation, Hagishita and Ohsaki [49] proposed an algorithm to allow adding and removing bars. Zegard and Paulino [50] uses both SIMP and GS methods to obtain optimal structural mechanisms for AM.

2.2   Infill optimization

In the context of the infill generation, there are different methods developed to optimize the component infill. Adaptive centroidal Voronoi tessellation was used to create a pore-based internal structure, and a strength-to-weight optimization is performed to obtain the minimum internal structure able to support a specific load [4]. Wu et al. [8] considered a bone-like optimized infill structure maximizing the mechanical stiffness using voxel-wise topology optimization. An infill generated by the optimization of the global stiffness under any load distribution is proposed by Wang et al. [5], based on the saddle point algorithm. Truss-like cellular structures can also be optimized using density information [51, 52]. Wu et al. [53] propose a method to create infill structures on rhombic cells. Steuben, Iliopoulos, and Michopoulos [54] proposed an implicit slicing algorithm. The generated toolpath is based on level sets of arbitrary heuristic-based or physics-based fields. Liu et al. [55] introduced a methodology to produce hybrid infill patterns based on level set principle. Void parts of the structure, where is under low stress, are filled with non-optimized patterns. Numerical examples are given. However, no physical tests were performed to demonstrate the mechanical strength of the obtained optimum design.

The aforementioned works are well established for topology optimization of infill generation, but they focus mainly on the geometry of the shape of the pattern. However, they do not take into consideration the properties of the toolpath-based AM process. For

example, the widely used FDM process [1] produces parts with anisotropic characteristics, demonstrated by the mechanical resistance of a component is lower when the load is applied perpendicularly to the filament orientation [6, 56, 57]. A similar result was obtained by Koch, Hulle, and Rudolph [58], where orientation, solidity, and edge effects were studied. Wittbrodt and Pearce [59] even found out that the filament pigment color could affect the component mechanical strength. These studies demonstrated that there is an influence of the filament orientation and conditions in the final component strength. Therefore, the toolpath planning should also take this influence into account.

Recently, the principal stress lines (PSL) has been applied in various domains. An important characteristic of PSL is that it is computationally fast. Therefore, it allows good interaction between the user and the optimization interface since the optimization result can be seen almost in real-time. Tam and Mueller [60] demonstrated the use of principal stress lines to deposit filament along the stress lines of the component. Using a six-axis robot arm, they were able to produce curved 3D surfaces directly. A topology optimization process based on PSL is also proposed by Kwok, Li, and Chen [11]. Their work demonstrates a good correlation with other topology optimization methods, as presented by Andreassen et al. [61]. However, these frameworks are based on the CAD model, and they did not consider the infill pattern of the part. The goal of this work is to apply the PSL technique in the slicing, such that the toolpaths are optimized for functional purpose as well. The computation efficiency of generating PSLs is an important characteristic when it is considered in the slicing process because it can generate a large number of layers.

3 Overview

The majority of structural optimization is done in the CAD development phase, but the toolpath-based AM processes have anisotropic characteristics, and thus the final property of part is also determined by how it is fabricated. This work proposes to apply topology optimization directly in the slicing operation. To achieve this goal, the optimization method must be fast, consider manufacturing parameters, and convert to machine instructions seamlessly. Due to the fact that a toolpath is a set of lines, it is preferred to employ a line-based topology optimization for toolpath planning. Recently, some TO research focuses on putting material to experience only the principal stresses so that there is no shear stress (shear modulus is normally smaller than Young's modulus). One way is to trace lines along the principal direction, which is called Principal Stress Line (PSL) [11]. PSL can be computed efficiently, and more importantly, it is represented in lines. Therefore, the PSL is applied in the toolpath planning, which takes not only the geometry information but also the manufacturing properties into account.

   For the conventional TO methods, the applied loads, boundary conditions, and structural information of the part should be inputted. However, to apply TO in the slicing, it means those information must be passed into the slicer, which is not user-friendly. Fortunately, the construction of PSL is based on the computation of principal directions, which requires only a stress field. The stress field can be represented by the stress values specified on each vertex and inputted to the system. It is possible because most common 3D printer file formats (e.g., AMF, 3MF, OBJ) can support the specification of textures or materials. The stress values in x-, y-, and z-axes can be stored as the r, g, and b colors, respectively. Therefore, the overall pipeline of the framework is as follows (as illustrated in Fig. 3.1):

(a) CAD domain   (b) Stress field   (c) 2D Plane slices

(d) Single plane PSL   (e) G-code output   (f) 3D printed component
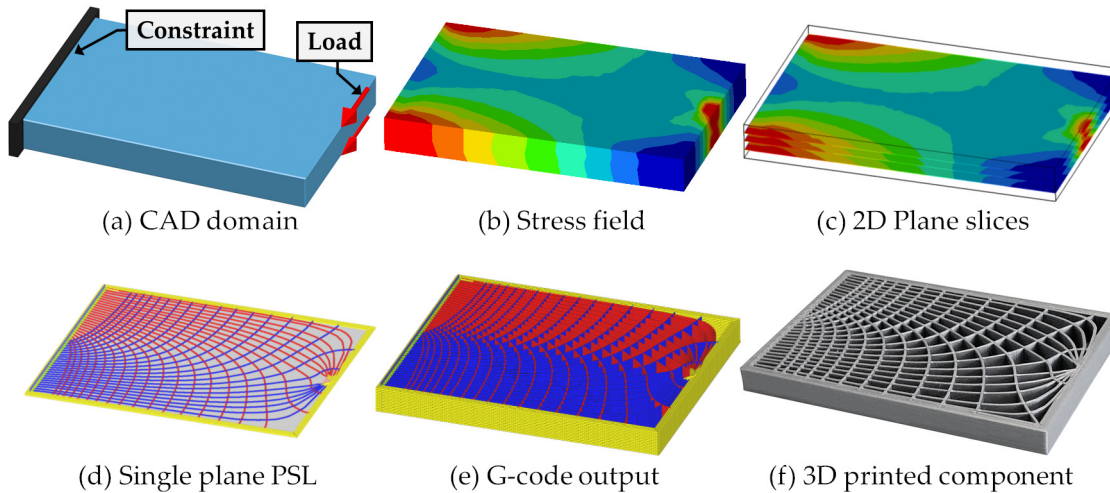
FIGURE 3.1: The framework overview for applying topology optimization in the CAM phase. (a) The initial domain containing boundaries conditions and loads. (b) The CAD model and stress field that are inputted into the CAM phase. (c) The model is sliced and the stress field is mapped onto each 2D plane. (d) The PSLs are generated in one single layer with the 2D stress field. (e) The PSLs can be readily converted to toolpaths as well as G-code for fabrication. (f) The 3D printed part.

1. With the defined loading conditions, the FEA is applied on a CAD model to compute a 3D stress field.

2. The CAD model, together with the stress field, is passed into the slicing software.

3. The model is sliced into a set of 2D planes, and the 3D stress field is mapped onto the planes getting 2D stress fields.

4. Within each 2D plane, PSLs are traced on the 2D stress field, satisfying the manufacturing requirements.

5. From the PSLs, the output will be the toolpaths (G-code) that can be directly fed to the AM machine for fabrication.

As a proof-of-concept, the method is implemented for an FDM 3D printer, but the framework could also be extended to other toolpath-based AM processes.

The steps of problem definition and analysis are standard as usual TO in the CAD phase, and the mapping of the 3D stress field to the 2D ones are similar to the one used by Steuben et al. [54]. The major difference is that they used the von Mises stresses (and thus the 3D-to-2D mapping eliminates the stresses in the z-direction) and this work uses
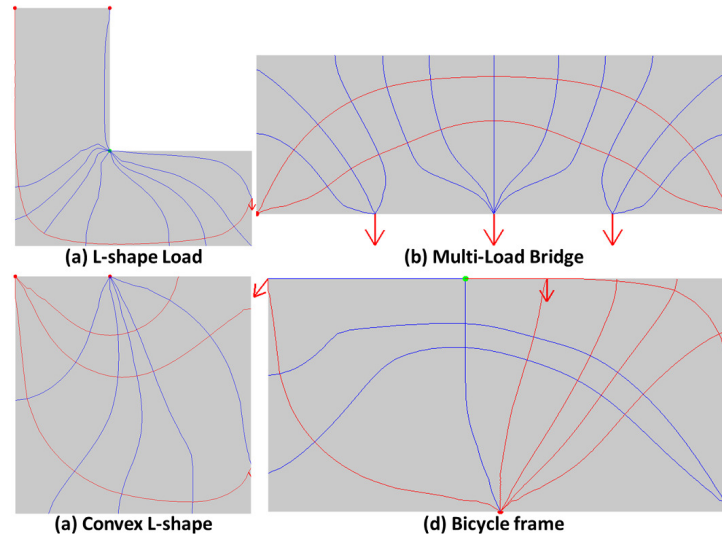
FIGURE 3.2: Examples of principal stress lines under different boundary conditions and loads [11].

the principal stresses. Therefore, the 2D stress field is assumed to be given in this work, and the concept is demonstrated with a layer of 2.5D shapes, which are 3D shapes with the same cross-sections along the height. It is also worth to mention that this work is different from 3D topology optimization. As most AM processes fabricate parts layer-by-layer, even the part is 3D topologically optimized, the toolpath planning in every single layer is still needed.

3.1   Design guidelines

Michell [62] studies state that a truss structure S under load Q is optimum if the truss members are exclusively under axial load. Therefore, the members are in tension or compression, minimizing the shear stress. Such principle means that the members of S follow the principal stress line [63] and justify the correlation between typical topology optimizations methods (e.g., SIMP) and the principal stress lines [60].

A typical continuous topology optimization problem can be presented as

$$\min_{\rho} \quad F = \int_{\Omega} f(\mathbf{u}(\rho), \rho) dV$$

$$\text{subject to} \quad g_0(\rho) = \int_{\Omega} \rho dV - V_0 \leq 0,$$

$$h_j(\mathbf{u}(\rho), \rho) \leq 0, j = 1, ..., m$$

where Ω is the problem domain, F is the compliance objective function, $\mathbf{u}$ is the state field, ρ is the element density, $g_0(\rho)$ is the inequality constraints, and $h_j(\mathbf{u}(\rho), \rho)$ is the equality constraints, that can be, for example, the maximum material mass or the maximum stress.

In this study, the selected optimization method is the principal stress lines. The design objective is to minimize compliance and obtain maximum stiffness. The design variables are the nodal coordinates and beam connections. The inputs are the 2D discretized domain, the stress field in the form of nodes displacement, and the desired infill ratio. The output is an optimized toolpath. Before giving the technical details of applying PSL for toolpath planning, the fundamental of PSL is presented first.

3.2 Principal Stress Line (PSL)

With a given domain $\Omega \in \mathbb{R}^2$ and a stress field, it is possible to obtain the stress tensor

$$\sigma = \begin{bmatrix} \sigma_{xx} & \tau_{xy} \\ \tau_{xy} & \sigma_{yy} \end{bmatrix}$$

where σ_{xx}, σ_{yy} and τ_{xy} are the stress components of p_i. The tensor defines the state of stress at a point $p \in \Omega$ and consequently the principal stress and principal angle for any specific point p_i.

The principal stresses can be obtained by

$$\sigma_{1,2} = \frac{1}{2} \left(\sigma_{xx} + \sigma_{yy} \pm \sqrt{(\sigma_{xx} - \sigma_{yy})^2 + 4\tau_{xy}^2} \right) \tag{3.2}$$

where σ_1 is the maximum principal stress, and σ_2 is the minimum principal stress. The principal direction θ_i of point p_i can be calculated by

$$\tan(2\theta_i) = \frac{2\tau_{xy}}{\sigma_{xx} - \sigma_{yy}}, \tag{3.3}$$

The principal stress line (PSL) is a line in which all segments are along the principal stress directions (Fig 3.2). Assume it starts from a seed point p_0 within the domain, the PSL can be traced by iteratively moving a small step along the principal direction until it exits the domain, and every subsequent point can be calculated using

$$p_{i+1} = p_i + \Delta \cdot \mathbf{v}(\theta_i), \tag{3.4}$$

where $\mathbf{v}(\theta_i)$ is a unit vector aligned with the principal angle θ_i and Δ is the increment size parameter. In this study, it is used $\Delta = 0.1\,\text{mm}$. As there are supposed to have two principal directions at each point, the one closest to the previous angle θ_{i-1} would be selected.

However, as it can be observed in Eq. 3.3, when σ_{xx} and σ_{yy} are equal, the principal direction is undefined. Kwok, Li, and Chen [11] used a strategy based on the optimal regions to make sure the structure is always generated in the well-defined regions. The optimal regions are classified into five types according to σ_1 and σ_2, but in this study they are grouped in three because of the symmetry in positive and negative values:

$$R: \quad |\sigma_1| > 0 \quad \text{and} \quad \sigma_2 = 0$$
$$S: \quad \sigma_1 = \sigma_2$$
$$T: \quad \sigma_1 > 0 \quad \text{and} \quad \sigma_2 < 0$$

Normally, the stresses would not be exactly zero, so $\sigma = 0$ commonly means that it is not significant, e.g., close to zero or very small compared to the other. In different regions, the stresses could run in only one direction (R), two directions (T), or all directions (S). The well-defined region is the T region, and more details could be found in [11]. Optimal regions for the wrench example are shown in Fig. 3.3.
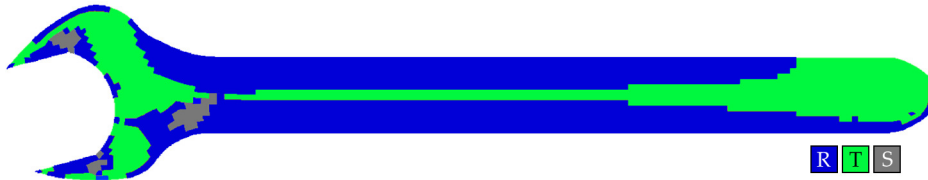
FIGURE 3.3: Different regions in the wrench example. R region is shown in blue, T region is shown in green and the S region in gray.

3.3 PSL-based toolpath

In theory, the PSLs should be as smooth as the underlying stress field is smooth. However, due to round-off errors and the resolution of the domain, there might be large variations in the principal angles between two consecutive points, especially in the transitions between different regions, resulting in irregular PSLs. The irregularity in some segments of PSLs does not affect much on the final structure, and they could always discard the irregular PSLs among the other good ones. Unfortunately, the smoothness requirement is much higher in this case, because all PSLs and every segment of them will be directly converted into the final toolpaths.

To make sure the computed PSLs are smooth, the tracing should consider not only the previous angle but also the optimal regions presented in Section 3.2. Therefore, different strategies need to be used in different regions. The *T* region is the good region with two well defined principal directions perpendicular to each other, and the tracing is the same as Eq. 3.4 with the one closer to θ_{i-1} is selected as θ_i. For the *R* region, there is only one principal direction, but indiscriminately using it as θ_i might result in a sharp turn for the PSL. This kind of PSL is not structurally sound, so the *R* region is treated the same as the *T* region, by adding another direction which is 90° different from the principal direction as the second principal direction. The *S* region does not allow the use of Eq. 3.3 to obtain the principal directions since σ_{xx} and σ_{yy} are equal. In this case, θ_i becomes undefined, and any direction is a valid direction. Therefore, the previous direction θ_{i-1} is used to calculate the next point p_{i+1}. The new tracing strategy based on different optimal regions can generate smooth PSLs, but there might still be some PSLs without structural meaning. For examples, a PSL is too small to be printed (e.g., a line

that is smaller than the nozzle diameter), or it is a duplicated line (e.g., overlapped with another line). These PSLs are eliminated to avoid printing errors and to reduce material waste. More details about the filtering method are presented in section 4.4.

When a PSL is concluded, a new PSL will be traced starting from the next seed point and the process is repeated until all seed points are computed. After all seed points are processed the PSLs are converted into toolpath and the toolpath walls are created with the offset of the domain internal and external borders. The toolpaths generated in this study are distributed uniformly and need to consider the manufacturing aspects as discussed in the following.

4 Methodology

As previously mentioned, an advantage of using PSL as an optimization strategy is that a PSL is formed by a set of nodes grouped in an organized way. Due to this characteristic, it can be converted to toolpath instructions (i.e., G-code) quickly using few computational resources, even in domains with a large number of elements. To perform the conversion, each PSL is read. The PSL nodes are converted to toolpath points, to preserve computational resources only position coordinates and node connections are preserved in the conversion. To generate the G-code, the toolpath points are exported, the first point as a $G0$ command and then $G1$ for all further nodes. The extrusion rate E is related to the amount of extruded material necessary and it is calculated using the distance between the nodes. Once a PSL is exported, this process iterates and the next nearest one is selected along the domain boundary, such that the nozzle travels along the perimeter avoiding any unwanted material added in the domain. With all PSL nodes converted, the order of the tool traveling is optimized. When a line is printed the closest point of the next line is selected to reduce the travel distance and printing time.

Although the conversion from PSL to toolpath is straightforward, there are several research questions that need to be answered. First, as the topologically optimized toolpaths are not regular, how to resolve the overlapping when the lines get close to each other? Second, how the PSLs should be constructed such that the infill ratio can be controlled? Third, when the PSLs are interlaced, how they should be printed so that the structural integrity of the final part is preserved? These questions are answered by the subsections.
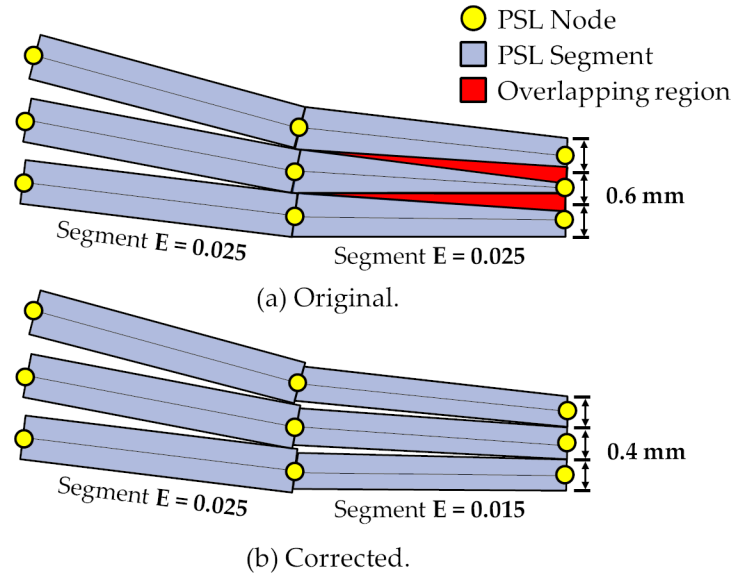
FIGURE 4.1: Controlling the extrusion rate to fix the line overlapping issues. (a) The initial line overlapping. (b) The lines with different extrusion rates.

4.1 Extrusion rate

Since the PSLs are generated based on the stress field, they tend to meet and concentrate in the regions with high stresses near constraints points. This agglomeration of material contributes to the redistribution of stresses so that the overall performance of the component is enhanced with the same amount of material. When the PSLs are getting dense, it is possible that excessive materials overlap between the lines occurs, Fig. 4.1(b). This behavior is similar to other non-uniform infill patterns [54]. The overlapping normally does not create failures in the fabrication process, but there may be possible consequences like discontinuous lines or reduced print quality due to the material scattering. Therefore, the overlapping should be avoided to ensure print quality and better use of material, making the most use of the intrinsic characteristics of PSLs and improving the optimization. A possible solution to line overlap could be a traditional closest point search routine, where a recursive smooth function would increase the distance between lines, or lines segments, as necessary to avoid the overlap. However, such approach can be computationally expensive and increase the material usage, since the new line position could be in a low-stress region without following the principal stress line.

Since the topology optimization is applied in the slicing, it is possible to solve the
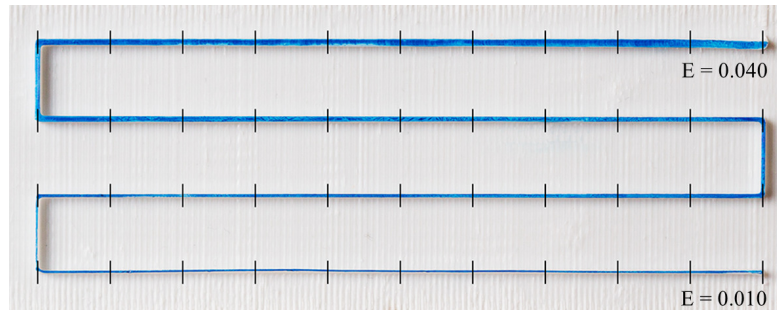
E = 0.040

E = 0.010

FIGURE 4.2: Extrusion rate test sample printed increasing the parameter *E* from 0.001 to 0.040.

problem in the toolpath planning as well. Recall that the extruder in an FDM printer is run by a sequence of *G1* linear move commands in the form of *G1 X80 Y77 Z4 E0.03*, where *X*, *Y*, and *Z* are the positions of the next point, and *E* is the extrusion rate, which specifies the amount of material (in mm) deposed while moving from one point to another.

By manipulating the value of parameter *E*, it is possible to control the extrusion rate and consequently the width of extruded material. In other words, the line width can actually be changing in a path during the printing process. A test sample was printed using an Ultimaker 3D printer with a g-code created using python. Therefore, no geometric slicing was performed to ensure complete control of the printing process. The material used is white PLA, the layer height is set to 0.2 mm, and the nozzle diameter is 0.4 mm. Blue ink was used to improve the line width visualization. A rectangular base 1.0 mm high was printed to provide support to the continuous line. The line has was printed increasing the value of *E* from 0.001 to 0.040 in 0.001 steps every 10.0 mm. The printed sample is shown in Fig. 4.2. It is possible to observe the increase in line width from the first segment ($E = 0.010$) to the last segment printed ($E = 0.040$). To allow an objective study, the line width of each segment is measured using a digital caliper.

The results of the measurement are shown in Fig. 4.3, where the horizontal axis is the Extrusion Rate *E*, and the vertical axis contains the line width, in mm. The line width is basically in a linear relationship with the extrusion rate. Therefore, a linear equation can be used to control the extrusion rate.
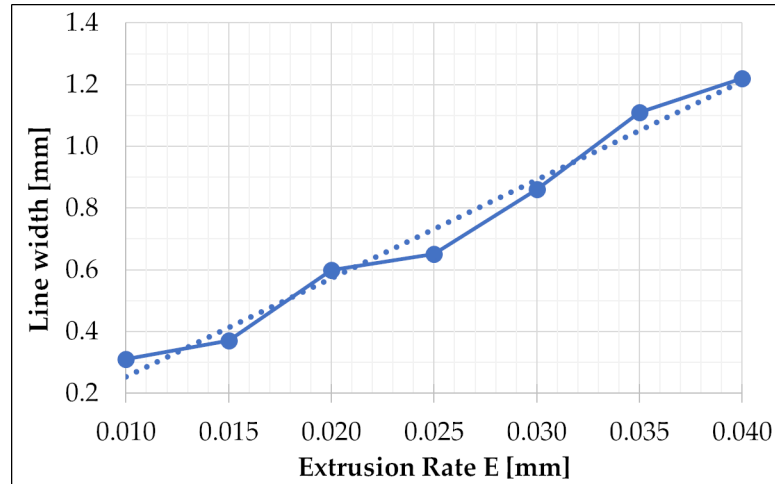
FIGURE 4.3: Relationship between line width and extrusion rate.

With this information, an algorithm is developed to allow the reduction of line over-lapping. Each PSL is checked with its neighboring PSLs to find if they have any overlapping segments. If there is, the maximum line width for each node is computed such that the lines segments only touch each other, considering the minimum line width allowable dimension, in this study, 0.2 mm. After that, the new line width is used to calculate the corresponding extrusion rate E at that particular segment. The new E value is associated with the line segment. Therefore, since the E value is individually specified for each line segment, a single toolpath line can have different line widths along its length.

Although changing the extrusion rate would complicate the calculation of the infill ratio (need to consider the width of each segment too), this method has the advantage of guarantee that the lines follow the principal directions, since the line nodes are not translated. Furthermore, it only needs to update the E values during the toolpath generation without introducing any additional control parameters. This can only be done because of applying topology optimization in the CAM phase. In this work, only the FDM printer is demonstrated. However, a similar methodology may also be applied for other toolpath-based additive manufacturing technologies.

4.2 Infill ratio

One attractive feature of AM processes is the capability of fabricating internal voids to minimize weight. Therefore, the CAM system for AM takes the infill ratio as one of the parameters, which controls the volume of material and porosity inside the part. The infill ratio can be easily fulfilled for uniform patterns by simply scaling the size of the unit cell to match with the material to void ratio. Although non-uniform infill patterns could have better stress redistribution and thus part performance than the uniform ones, the same principle to control infill ratio for the uniform does not apply for the non-uniform. For example, Steuben, Iliopoulos, and Michopoulos [54] introduced a scalar parameter in the implicit function to control the infill ratio, but they did not mention how to set it to achieve a certain ratio. The PSL-based infill pattern is also non-uniform, and the length of each PSL is unpredictable. Fortunately, the PSL computation is very fast, and a search method to find the right seed density to obtain the desired infill ratio can be developed.

A PSL is traced from a seed point on the external domain boundary. Thus, controlling the number of seed points can cause a variation in the number of PSLs generated. Consequently changing the amount of infill. The goal is to find the number of seeds necessary to fulfill the requested infill ratio value. Assume there are n seeds $s = \{s_i, i = 1, 2, ..., n\}$ distributed uniformly along the domain boundary separated by a distance of $\Delta_d = l/n$, where l is the total length of the boundary.

The relationship between the number of seeds and infill ratio is demonstrated visually in two different examples. The first example is the Symmetric Cantilever domain, shown in Figure 4.4. The three different desired infill ratios used as input are 25.0%, 50.0% and 75.0%. Varying the number of seeds, the obtained infill ratios for this example are 25.2%, 52.3%, and 72.4%, with 25, 50, and 75 seeds respectively. The maximum error between desired and obtained infill is 4.4% in the 50.0% desired infill. The second example, shown in Fig. 4.5, uses the L-Shape domain and considers the same desired infills as input. For this example, the obtained infill results are 25.4%, 52.2%, and 72.0% with 25, 50, and 75 seeds respectively. The same study is also performed in

Cantilever (sym.) Domain   Infill R.: 25.2%, Seeds: 25.

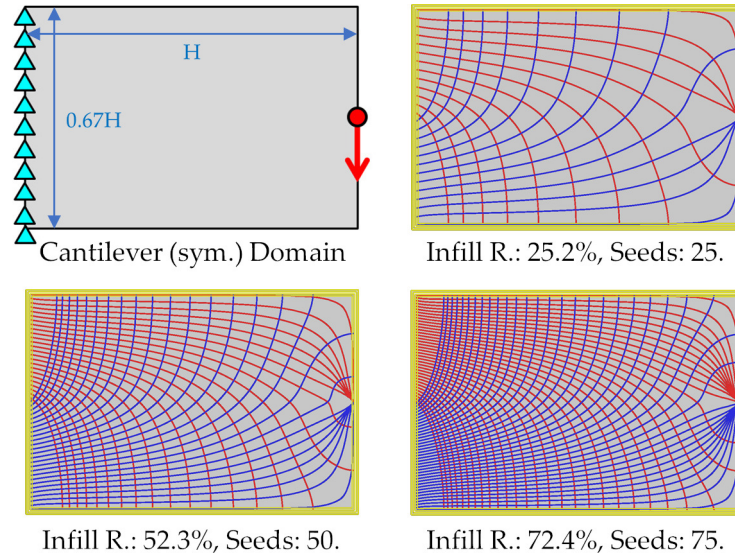Infill R.: 52.3%, Seeds: 50.   Infill R.: 72.4%, Seeds: 75.

FIGURE 4.4: Three different infill ratios for the symmetric cantilever example varying the number of seeds from 25 to 75.

Symmetric Cantilever and Bridge domains. The different results are combined in Figure 4.6. It shows the relationship between the infill ratio and the number of seeds necessary to obtain the desired infill for different domains. It can be seen that with the increase in the number of seeds, the infill ratio is increased monotonically.

With this observation, an optimization is presented in Algorithm 1, in which the desired infill ratio (I) is the input and the output is a set of PSLs, i.e., $PSL = Infill(I)$. Basically, it is a binary search method, starting from the average value between the maximum and the minimum number of seeds and incrementally increasing or decreasing to get the optimal value. The maximum value depends on the length of the boundary and the size of the nozzle, while the minimum value could be zero. To avoid an infinite loop, the maximum number of interactions is controlled by the parameter max_steps. The end condition is when the difference between the desired infill ratio I and the obtained infill ratio i is lower than max_error. In this work it is considered $max\_error = 5\%$. This algorithm calls two functions: GENERATESEEDS(n) generate seeds uniformly along the outer domain boundary. The seeds are used in the function GENERATEPSL(S) to generate the PSLs as described in Chapter 3.
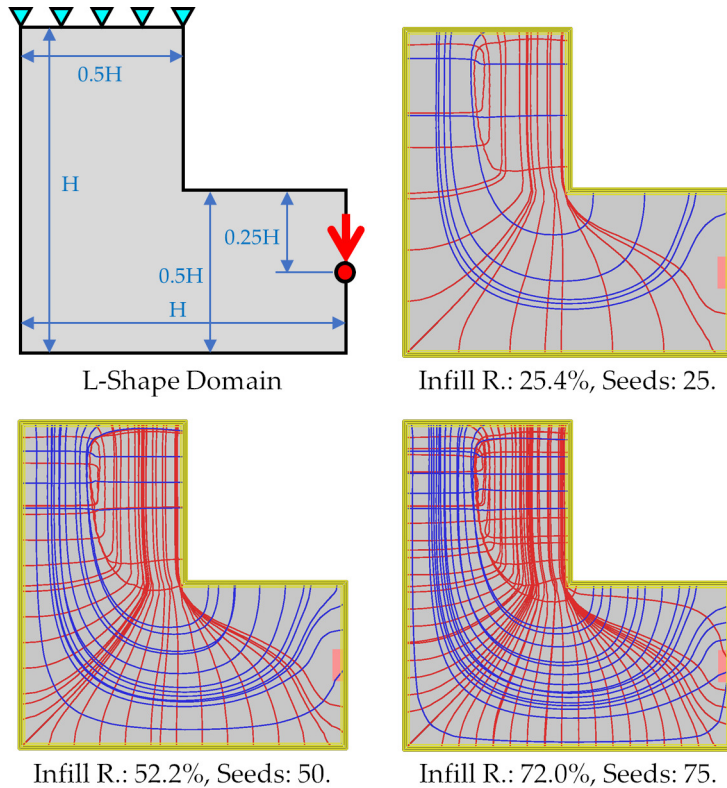
FIGURE 4.5: Three different infill ratios for the L-Shape example varying the number of seeds from 25 to 75.

4.3 Tension and compression analysis

When the infill patterns generated by the common CAM software are interlacing like the grids, triangles or cubic, the printer normally prints one direction first and then other directions by crossing over the previously printed ones. This crossover is acceptable as the intersections are small, and it is also preferred as the structural integrity of the lines is preserved better compared to making stops at each intersection. While the crossover has been done randomly in the existing software, it is possible to optimize further the order of printing the PSLs for enhanced properties due to the additional information provided by the stress field. Again, the FDM process is discussed here, but a similar procedure might be applied to other processes.

In an FDM machine, when there are two paths intersecting each other in the same layer, the first one will be printed as usual and the second one will be blocked by the first one resulting in a weak connection at the intersection point. Although it may not have
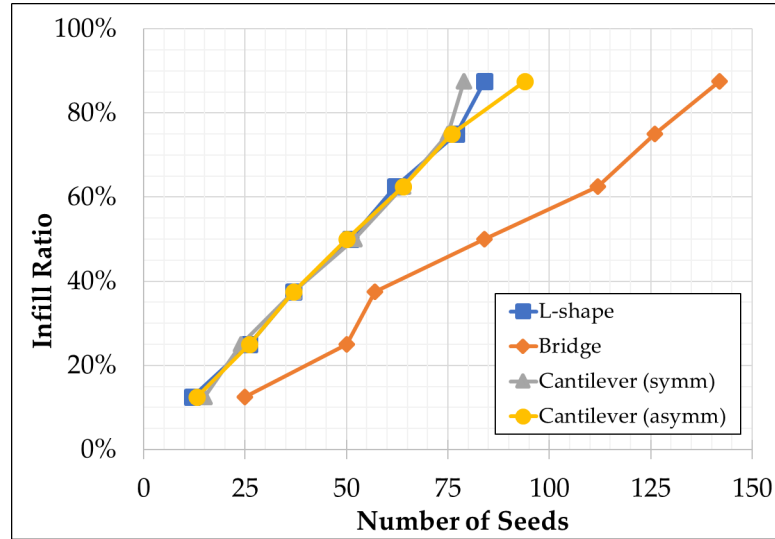
FIGURE 4.6: Relationship between infill ratio and the number of seeds for different domains.

a significant effect on the PSL's performance with compressive loads, this discontinuity in the printed line will decrease the segment strength when tensile loads are applied. To avoid such weakening, it is necessary to ensure as many lines under tensile load as possible are printed with the lowest number of discontinuities. Thanks to the given stress field, it is possible to classify the PSLs into two different groups: *tensile* and *compressive* PSLs. The classification is obtained using the minimum or maximum principal stress correlated with the principal direction θ_i obtained for each PSL point p_i, as described in Chapter 3. The average stress of all points contained in the PSL is calculated. If the average stress $\sigma_a \geq 0$, the PSL is classified as compressive PSL, otherwise as tensile PSL. This data is very useful in the toolpath planning, since it can be used to improve the mechanical properties of the part.

Two specimens with the exact same infill pattern are fabricated, but one has a random printer order of the PSLs, and the another one follows the classification. They have the same weight and are tested with the same condition (the cantilever case in Fig. 3.1). The maximum load supported by the test specimen considering compressive/tensile classification was 39.40 kgf. For the one printed randomly, the maximum load was 33.84 kgf. Therefore, with the application of PSL classification, using the average stress in each line, it was possible to increase the mechanical strength of the test sample by

---

Algorithm 1 Infill Ratio Binary Search

1: **function** INFILL(I)
Require: $0 < I < 100$
2:     $n_l \leftarrow n_{min}, n_r \leftarrow n_{max}, n \leftarrow (n_l + n_r)/2$ ▷ for search
3:     **for** $k = 0$ to *max_steps* **do**
4:         $S \leftarrow$ GENERATESEEDS(n)   ▷ Generate seeds uniformly
5:         $PSL \leftarrow$ GENERATEPSL(S)   ▷ Generate PSLs
6:         $i \leftarrow (V(PSL)/V(total)) \times 100$ ▷ Infill ratio
7:         **if** $abs(I - i) > max\_error$ **then**
8:             **if** $i < I$ **then**
9:                 $\Delta_{seed} \leftarrow abs(n_l - n)/2$
10:                 $n_l \leftarrow n;$
11:                 $n \leftarrow n + \Delta_{seed}$ ▷ Increase seed count
12:             **else**
13:                 $\Delta_{seed} \leftarrow abs(n_r - n)/2$
14:                 $n_r \leftarrow n;$
15:                 $n \leftarrow n - \Delta_{seed}$ ▷ Decrease seed count
16:             **end if**
17:         **else**
18:             **return** PSL ▷ Return PSLs
19:         **end if**
20:     **end for**
21: **end function**

16.4%. To generate the final toolpaths, a data structure was created with three groups. Besides the two groups of compressive and tensile PSLs, another group is the toolpath for the walls, i.e., domain boundary. The order in printing them is firstly the *Tensile PSLs*, followed by the *Compressive PSLs* and finally the *Walls*. This configuration allows printing the tensile PSLs in continuous lines. Since there are intersections between different groups, the compressive PSLs are less affected by the discontinuities. The wall group is the last to increase the mechanical strength of the bond between the wall and the infill (PSLs).

4.4 PSL filtering

As mentioned in Chapter 3, it can occur that a PSL enters a region with degeneracies in the stress tensor. These regions are treated as specified in Section 3.2. However, it is still possible to obtain irregular infill which may not have structural function [11]. For
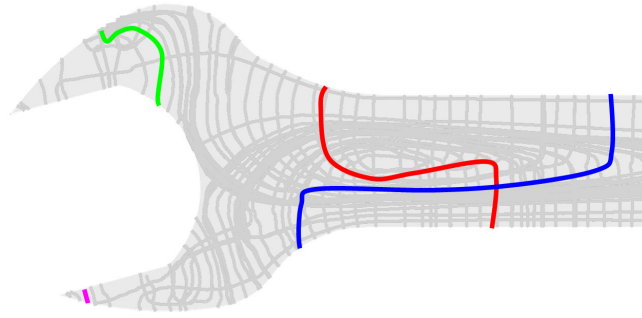
FIGURE 4.7: Irregular toolpath in wrench example.

examples, infill lines with a length smaller than the line width, lines which return to their original position and lines with self-intersection. Some examples of irregular lines are shown in Fig 4.7. Those infill lines are identified and filtered automatically in the toolpath generation procedure to avoid material waste. They are also excluded from the final infill calculation. Figure 4.8 shows valid and invalid PSLs in the wrench example after the application of the filtering process. Therefore, despite the uniform initial sampling, the final seed distribution is non-uniform, as shown in Fig. 4.8(a). Below a summary of all PSL filters used in this framework.

a) PSL length: based on the total PSL length, the PSL is considered invalid if the PSL total length is lower than three times the nozzle diameter.

b) PSL number of segments: the PSL is considered invalid if the number of segments in the PSL is lower than two.

c) PSL average stress: the PSL is considered invalid if the average PSL stress is lower than 10% of the maximum stress in the domain.

d) PSL proximity: the PSL is considered invalid if while tracing a PSL from a seed point, its endpoint end at/around another seed point(s) on the boundary. Those seed points that are close to existing PSLs will be removed to avoid duplication of PSLs. A seed point and a PSL end point are considered close when the distance between these points is smaller than two times the line width.

(a) Valid PSL

(b) Invalid PSL
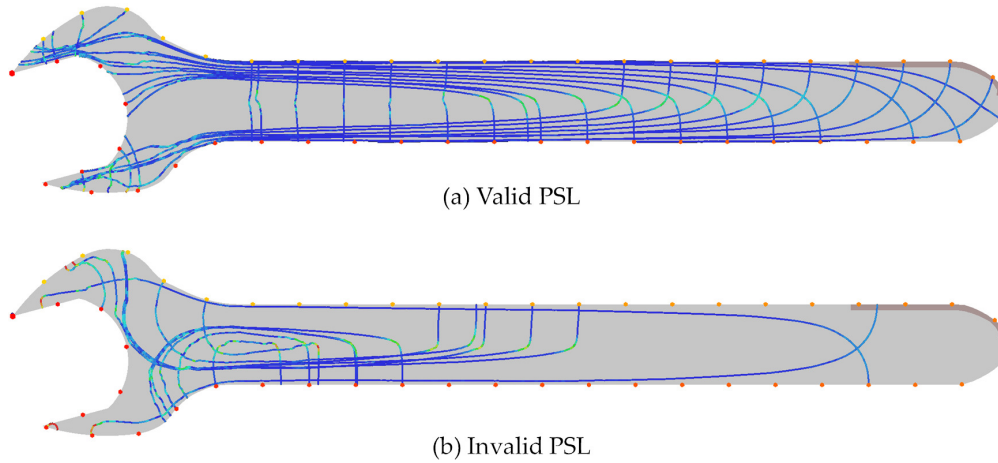
FIGURE 4.8: Filtered PSLs in wrench example. (a) Shows the valid lines. (b) Shows the filtered invalid lines, these lines are not considered in the infill calculation.

e) PSL curve angle: This filter considers the ratio between angle variation and segment length. It avoids acute curves. The PSL is considered invalid if the ratio between angle variation and segment length is greater than 30.

5 Results

The proposed framework is implemented with VC++ and tested numerically and physically, the results of which are presented in this chapter. As mentioned in Chapter 3, most AM processes fabricate parts layer-by-layer, and toolpath planning in a single layer is necessary no matter the 3D shape is optimized or not. Therefore, this work focuses on the toolpath generation on a 2D plane with a given 2D stress field. All the tests are run on a computer with Intel Core I7-3770K @ 3.50GHz, 32GB of RAM and Windows 7 64bits. The PSL infills will be compared with other infills first. Then the presented method will be applied in various domains, and the time statistics will be reported.

5.1   Comparison with other infills

To verify the method in enhancing part strength with the same material used, the cantilever problem shown in Fig. 3.1 is studied. In this example, a 2D rectangular domain is employed, in which the fixed boundary conditions are applied at one end, and a load is applied at the middle of the other end. The stress field is visualized in Fig. 3.1(c), and the high stresses are located near the constraints, indicated by the red color. The toolpath visualization in Fig. 3.1(d) indicates that all infill toolpaths generated in the upper part of the domain are in the tensile group (red), while the bottom ones are in the compressive group (blue). This result indicates that the PSL classification, presented in section 4.3, is working as expected since the downward load will generate compressive stress on the bottom of the domain and tensile stress on the top of the domain. The same behavior can be observed in other examples.

To compare these results, three other uniform infills commonly used by commercial software (e.g., Cura) are generated: Triangle, Tri-hexagon, and Grid (Fig. 5.1). The

(a) PSL   (b) Triangle

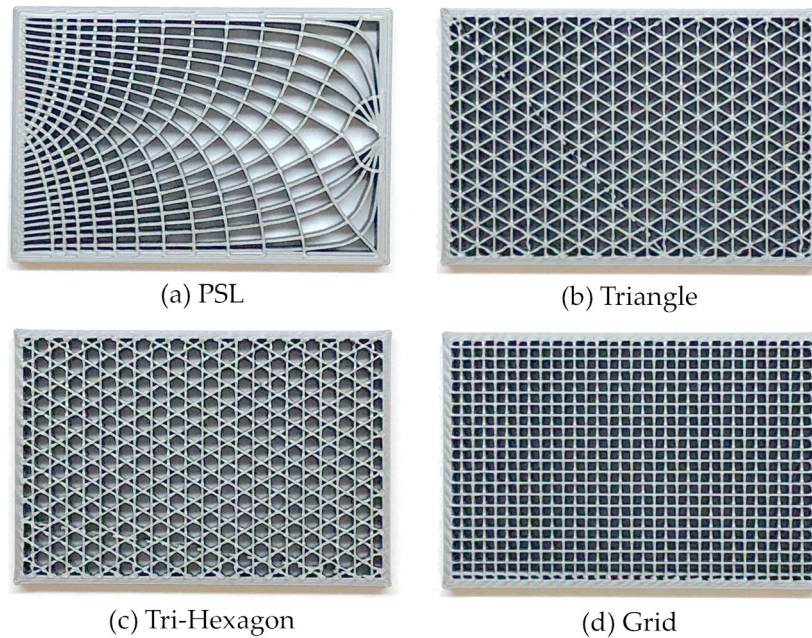(c) Tri-Hexagon   (d) Grid

FIGURE 5.1: Four infill patterns used for comparison. (a) The proposed PSL pattern generated using this framework, and (b)-(d) are the uniform patterns created by commercial software. All samples have the same mass and were printed with the same material in the same machine.

infill ratio for all cases is set to 45%. Firstly, they are compared numerically using the finite-element method and the fracture analysis. A finite element model was created for each infill with one single layer using exclusively beam elements. The boundary conditions applied are the same as in Fig. 3.1(a). All models are made sure using the same amount of material. The walls have a width of 1.2 mm, and the infill line width is 0.4 mm. To find the stresses, Nastran with solution 101 is used. During the iterations, elements with high compressive or tensile stress ($\sigma_u > 27$MPa) were removed from the model to simulate the fracture growth. The results are shown in Fig. 5.2, in which only the Triangle pattern is shown as a representative of the uniform infills because the Tri-Hexagon and the Grid have very similar fracture results occurring in the same way and in the same region. For the uniform infills, the fracture always occurs in the region near the constraints, where the highest stresses concentrate on this cantilever configuration, the fracture keeps propagating, from top to bottom, around the high-stress region along a straight line. Different from the non-optimized infill, the PSL toolpath has a more uniform stress distribution and the fracture starts from a line around the middle
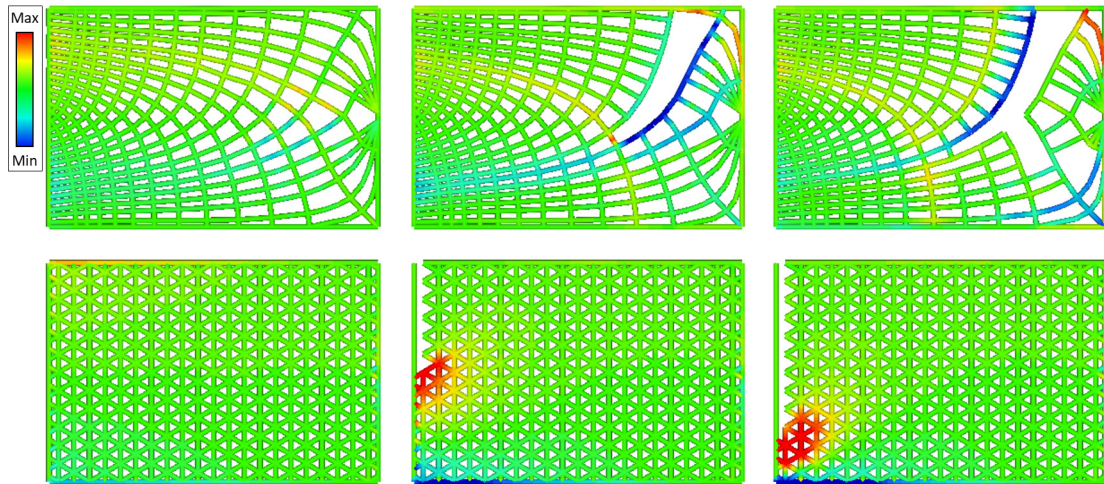
FIGURE 5.2: Finite element and fracture analysis comparison between the PSL and the Triangle infills, maximum principal stress plot. Stresses higher than the material tensile ultimate stress are shown in red. The PSL infill shows a stress redistribution during the fracture, while the triangle infill has high-stress concentration along the left boundary.

of the domain rather than the boundary conditions. The fracture propagates in a curved shape and in a different direction, and there are even fractures occurred in another position that is disconnected with the previous one. These results demonstrate that the PSL infill can channel the stresses from the highly concentrated region to other regions, and redistribute the stresses when a fracture occurs, allowing better structural performance.

Physical tests were performed to validate the results. All test samples were printed on an Ultimaker 3 FDM 3D printer using the same material batch. The selected material was silver polylactic acid (PLA). The layer height used was 0.20 mm and the test specimens size was $40mm \times 60mm \times 5mm$. Top and bottom surface were disabled to allow easy visualization of the infill and failure mode. The samples were weighed to confirm that they have the same amount of material. The fabricated test specimens are those in Fig. 5.1(a)-(d).

The experiments were realized in a Mark-10 tensile tester machine, as shown in Fig. 5.3. The force was measured by a load cell connected to the data acquisition system. The tests were performed until the complete fracture of the component (Fig. 5.4). Confirming the results of the numerical simulation, all the uniform infills were broken by the edge along the boundary conditions, while the PSL infill is fractured around the
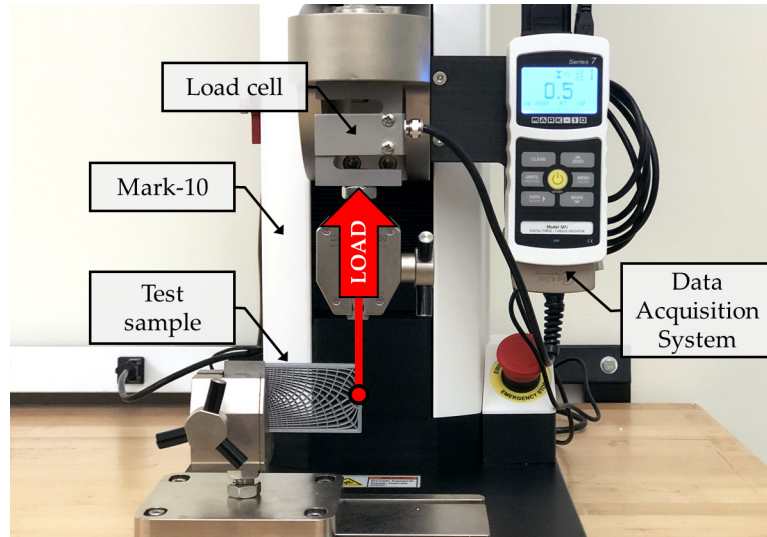
FIGURE 5.3: The physical experimental setting for the destructive tests.

TABLE 5.1: Experiment results between different infills.

Specimen	Infill	Max. Load [kgf]
a	PSL	39.40
b	Triangle	25.36
c	Tri-Hexagon	26.97
d	Grid	26.22

center. The result values reported in Table 5.1 are the maximum load sustained by each of the test specimens. All tests were realized under the same boundary conditions.

As we can observe, the test specimen with the PSL infill generated by this framework has the best result, supporting a force of 39.40 kgf, an increase of 55.3 % when compared with the Triangle infill. It is important to remind that the only difference between the PSL and the other test specimens is the structure utilized in the infill.

5.2 Other examples

The proposed method is also demonstrated with various boundary conditions, as shown in Fig. 5.5. For each of the domain, a stress field was computed in 2D by the given loads. Using the framework, the PSLs were then generated with a target infill around 50%, converted to toolpath and the wall lines created. Different toolpath groups are differentiated by the colors shown in the last column of Fig. 5.5. The yellow lines indicate the

(a) PSL   (b) Triangle

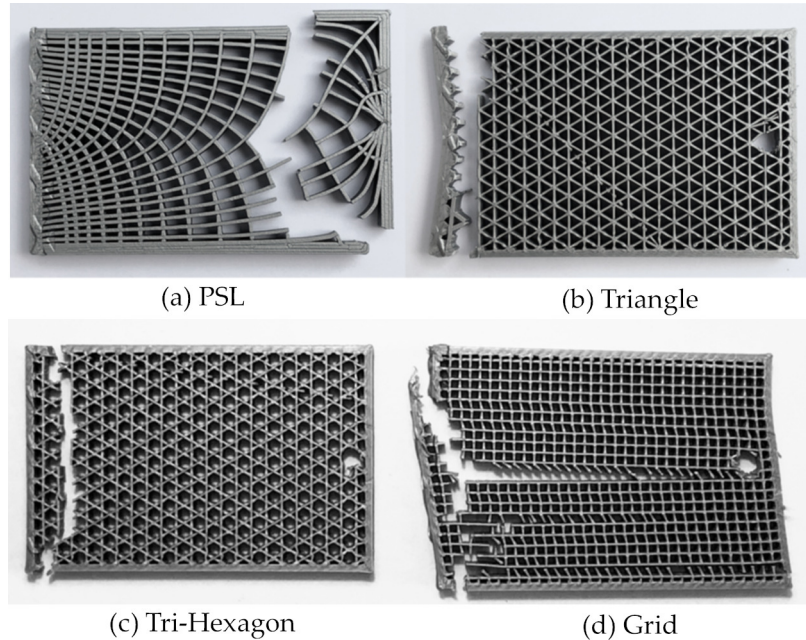(c) Tri-Hexagon   (d) Grid

FIGURE 5.4: Destructive test results of the cantilever case. (a) The PSL test sample. (b) The triangle test sample. (c) The tri-hexagon test sample and (d) The grid test sample.

wall group, the red ones indicate the toolpath of the tensile group, and the blue ones indicate the toolpath belonging to the compressive group.

The first row in Fig. 5.5 is an asymmetric cantilever problem with the downward load at the bottom-right of the domain. The stress field shows that it can account for the difference in stress distribution compared with the symmetric case. The toolpaths generated by this method conform well with the results presented by the 3D infill optimization method [8], but with a higher resolution. It can be seen that the proposed framework can work for both symmetric and asymmetric cases without modifying the method. The second example in Fig. 5.5 is a typical bridge case with one constraint in each lowest corner of the domain. The load is applied in the horizontal center at the bottom of the domain. The constraint and load regions present the highest stresses. The compressive PSLs forms an arc to connect the supports, while the tensile lines connect the compressive line to the point of load.

To demonstrate this method, more complex examples are studied. In a combustion engine, a connection rod is used to connect the piston to the crankshaft. One of it mains function is to transfer the downward load which occurs on the top of the piston during
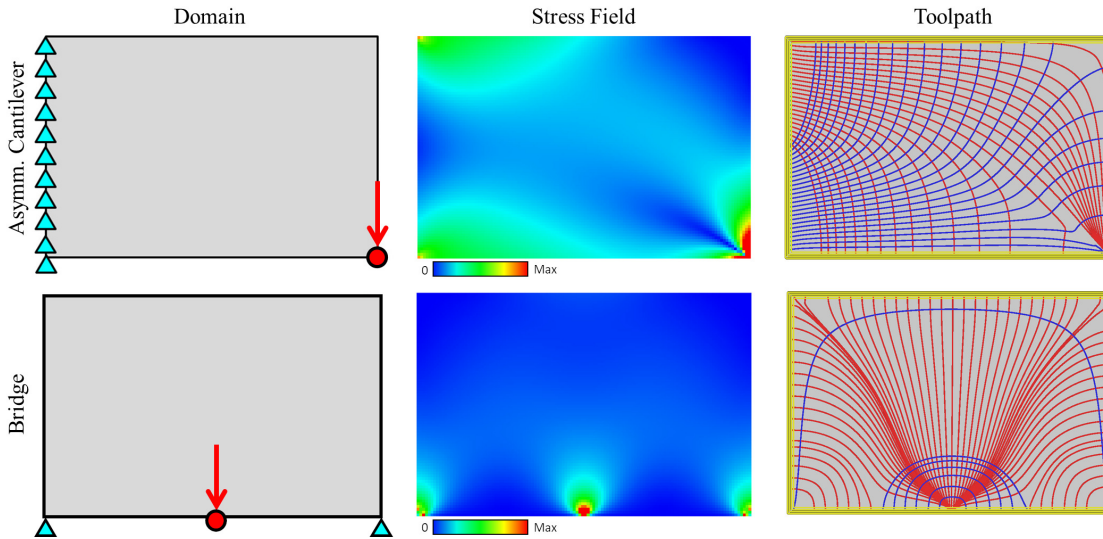
FIGURE 5.5: Asymmetric cantilever and bridge examples. The first column shows the initial domain containing boundaries conditions and loads. The second column contains the computed stress field. The last column shows the generated toolpaths.

the combustion stroke, translating the linear motion into rotational motion. A study using a connection rod base (Fig. 5.6) is performed. The CAD model was exported, then sliced and a stress field generated. A downward load is applied in the interface region between the connection rod base and the piston pin, indicated by red arrows in Fig. 5.6(b). The bottom region is constrained, simulating the contact with the crankshaft. The seeds are generated uniformly in the outer border. PSL is generated for each seed and filtered. Finally, the outer and inner walls are created and the PSL converted into toolpath, Fig. 5.6(d). The toolpath is well distributed, with vertical and horizontal lines.

Figure 5.7 shows the results for a typical 17 mm wrench tool. The same procedure shown in the previous examples is used. The geometry is created using CAD software and exported to this framework. It is sliced to generate the stress field and the toolpath is generated. As we can observe, the stress field in Fig 5.7(b), shows four regions with high-stress concentration (shown in red). To improve mechanical performance, these regions must be filled with material. Figure 5.7(c) shows the final toolpath. The seeds are originally distributed equally around the outer domain border. For each seed, a PSL is generated. Using the filtering proposed in section 4.4 some lines are excluded. After this step, the seed distribution is not uniform anymore. The high-stress regions are filled

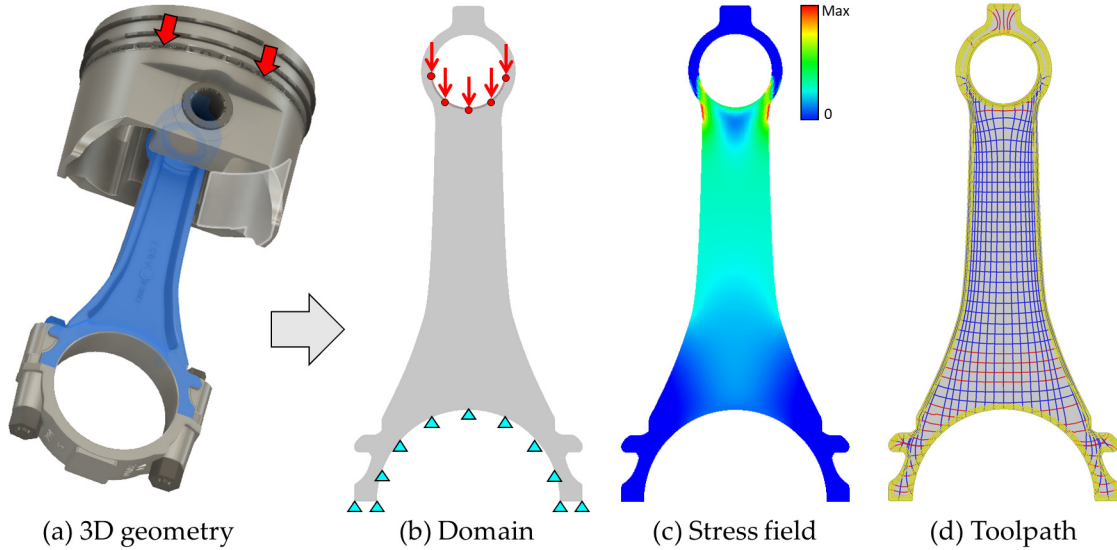(a) 3D geometry   (b) Domain   (c) Stress field   (d) Toolpath

FIGURE 5.6: Piston connection rod example. (a) The connection rod 3D model. (b) Shows the initial domain containing boundaries conditions and loads. (c) The computed stress field. (d) Generated toolpaths.

TABLE 5.2: Time statistics for the PSL-based toolpath planning. #Ele is the number of elements in the domain, t_{total} is the total time with the binary search, and t_1 is the time for one iteration.

Domain	#Ele	t_{total} [s]	t_1 [s]
Bridge	9600	1.283	0.272
Cantilever (sym.)	9600	0.221	0.221
Cantilever (asymm.)	9600	0.963	0.290
Piston Connection Rod	16751	2.661	0.608
Wrench	11482	4.372	0.229

with material following the principal stress direction.

5.3 Time statistics

Since a 3D model can have a large number of layers, the time expense to generate the PSLs per layer is extremely important for the practical use. Table 5.2 shows the time results for different types of domain. The column t_{total} contains the time necessary to perform all infill interactions to obtain the desired infill, column t_1 shows the time to calculate all PSLs for one layer. The t_1 is depending on the PSL step size Δ as well as the desired infill ratio. Higher infill values tend to demand a higher number of seeds, and therefore the computation time will increase. In the symmetric cantilever problem,

(a) 3D geometry

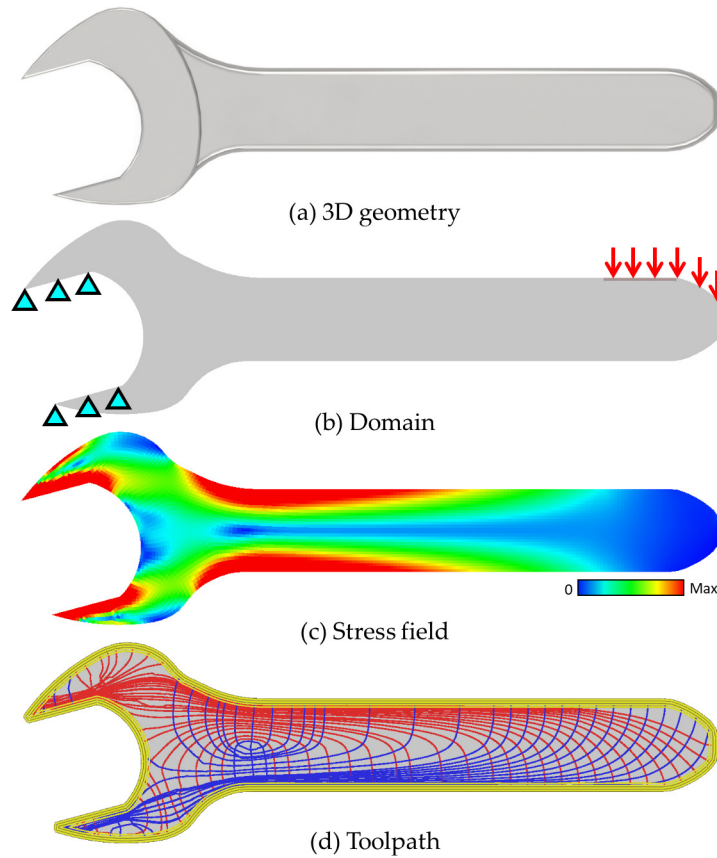(b) Domain

(c) Stress field

(d) Toolpath

FIGURE 5.7: Wrench example. (a) The 3D geometry. (b) The initial domain containing boundaries conditions and loads. (c) The computed stress field. (d) The generated toolpath.

the time spend to generate PLSs with 50 seeds was $0.221s$. Increasing the infill ratio to 75%, 75 seeds were needed to obtain the requested infill, and consequently, the time increased to $0.383s$.

To compare the results with other TO methods, it was used the MATLAB code from [21] to run the SIMP method and [34] for the Level-Set method. The selected test case was the asymmetric cantilever. The mesh size for all methods was 120×80 and the infill ratio is 50%. The convergence time is $1466s$ for the Level-Set method, $37s$ for the SIMP method and $0.963s$ for this method. The time statistics reported for the Level-Set and SIMP methods only consider the optimization time, without the extra time necessary to convert their results to toolpath. This result shows that this PSL-based method is much more ready to be applied for toolpath planning compared with other methods.

6 Conclusion

This work demonstrates a new toolpath planning methodology by considering both design and manufacturing requirements. It is a line-based topology optimization so that it can be readily converted into toolpath for fabrication. The obtained results demonstrated the influence of the optimized toolpath in the component mechanical strength. A 2D slice is given with a stress field, and an optimized toolpath can be generated using principal stress lines (PSL).

The use of PSL, as an optimization tool, also demonstrates that it is fast and reliable, generating good results. The results obtained demonstrate an increase in mechanical strength when compared with regular infill produced by commercial software. The optimized component generated by this framework using PSL was 55.3% stronger in the ultimate load. Using the stress field, PSLs can be classified as compressive or tensile. The classification allows further optimization of the printing order. Tensile lines were printed first to avoid discontinuities. PSL classification increased the test sample mechanical strength by 16.4% when compared with a test sample without classification. To reduce material overlapping, a method for toolpath planning was developed. By controlling the amount of extruded material, it was possible to vary the line width of a path. A study was performed to obtain the relationship between the extrusion rate E and the line width. The non-uniform infill generated by PSL as an advantage is that it can redistribute the stresses, but as a limitation is that the non-uniformity makes it difficult to control the infill ratio. Using the binary-search algorithm presented in this work, it is possible to obtain some desired infill ratio. However, if the infill ratio is very high, for example, 100%, there might be voids between different PSLs. A possible solution to obtain high infill ratios would be the use of a hybrid infill, in which empty areas would be

filled with uniform infill types, such as grid, triangle or lines. The disadvantage of this approach would be the creation of disconnected lines inside the domain, which is not structurally sound. Fortunately, high infill ratio is not commonly used for 3D printed parts.

There are some limitations and future works. In the current implementation, this framework considers a 3D model as multiples 2D layers and only the individual 2D slices were demonstrated. Further work is necessary to extend to real 3D cases fully. For example, while planning toolpaths in a layer, the previous layer has to be taken into account, so that the printing is always self-supported. It would be accomplished with seeds located in 3D surfaces or inside the 3D domain, instead of the sliced 2D domain border. The toolpath created should consider the use of robotic or 5-axis 3D printer and a new path planning strategy. Other sampling strategies would be studied to find the best seed distribution without depending on filtering. It would reduce the processing time since unnecessary PSLs would not be generated, avoiding computational resources waste. Furthermore, seed distribution would also be performed inside the domain, with seeds being created in the high-stress regions. This approach would guarantee that high-stress regions would always have material added via PSL.

Bibliography

[1] D. L. Bourell. "Perspectives on Additive Manufacturing". In: *Annual Review of Materials Research* 46.1 (2016), pp. 1–18.

[2] T. Alani, F. Othman, and H. Ali. "Effect of infill Parameter on compression property in FDM Process". In: *Int. Journal of Engineering Research and Application* 7 (Oct. 2017), pp. 2248–962216.

[3] K. Alvarez, R. Lagos, and M. Aizpun. "Investigating the influence of infill percentage on the mechanical properties of fused deposition modelled ABS parts". In: *Ingeniería e Investigación* 36 (Dec. 2016), pp. 110–116.

[4] L. Lu et al. "Build-to-last: strength to weight 3D printed objects". In: *ACM Transactions on Graphics* 33.4 (July 2014), pp. 1–10.

[5] T. Y. Wang et al. "Global Stiffness Structural Optimization for 3D Printing under Unknown Loads". In: *Journal of Computer Graphics Techniques (JCGT)* 5.3 (Aug. 2016), pp. 18–38. ISSN: 2331-7418.

[6] S. Ahn et al. "Anisotropic material properties of fused deposition modeling ABS". In: *Rapid Prototyping Journal* 8 (Oct. 2002).

[7] B. Rankouhi et al. "Failure Analysis and Mechanical Characterization of 3D Printed ABS With Respect to Layer Thickness and Orientation". In: *Journal of Failure Analysis and Prevention* 16 (May 2016).

[8] J. Wu et al. "Infill Optimization for Additive Manufacturing—Approaching Bone-Like Porous Structures". In: *IEEE Transactions on Visualization and Computer Graphics* 24.2 (Feb. 2018), pp. 1127–1140.

[9]   J. Haslinger and R. Makinen. *Introduction to Shape Optimization - Theory, Approximation, and Computation*. Society for Industrial and Applied Mathematics, 2003. ISBN: 978-0-89871-536-1.

[10] M. P. Bendsøe and O. Sigmund. *Topology Optimization: Theory, Methods, and Applications*. Berlin: Springer, 2003.

[11] T. H. Kwok, Y. Li, and Y. Chen. "A structural topology design method based on principal stress line". In: *Computer-Aided Design* 80 (Nov. 2016), pp. 19–31.

[12] G. N. Vanderplaats. "Thirty years of modern structural optimization". In: *Advances in Engineering Software* 16.2 (1993), pp. 81 –88. ISSN: 0965-9978.

[13] R. T. Haftka and J. Sobieszczanski-Sobieski. "Structural Optimization: History". In: *Encyclopedia of Optimization*. Ed. by Christodoulos A. Floudas and Panos M. Pardalos. Boston, MA: Springer US, 2009, pp. 3834–3836.

[14] K. Svanberg. "Structural optimization". In: *Encyclopedia of Optimization*. Ed. by Christodoulos A. Floudas and Panos M. Pardalos. Boston, MA: Springer US, 2009, pp. 3832–3834.

[15] L. A. Schmit. "Structural synthesis 1959-1969-A decade of progress". In: (1971).

[16] Y. Ding. "Shape optimization of structures: a literature survey". In: *Computers & Structures* 24.6 (1986), pp. 985 –1004.

[17] O. Pironneau. "Optimal shape design for elliptic systems". In: *System Modeling and Optimization*. Ed. by R. F. Drenick and F. Kozin. Berlin, Heidelberg: Springer Berlin Heidelberg, 1982, pp. 42–66.

[18] R. M. Hicks, E. M. Murman, and G. N. Vanderplaats. "An assessment of airfoil design by numerical optimization". In: (Jan. 1974).

[19] Z. Lyu, G. K. W. Kenway, and J. R. R. A. Martins. "Aerodynamic Shape Optimization Investigations of the Common Research Model Wing Benchmark". In: *AIAA Journal* 53.4 (2015), pp. 968–985.

[20] H. Xiaolong et al. "Robust aerodynamic shape optimization—From a circle to an airfoil". In: *Aerospace Science and Technology* 87 (2019), pp. 48 –61.

[21]   M. P. Bendsøe and N. Kikuchi. "Generating optimal topologies in structural de-
        sign using a homogenization method". In: *Computer Methods in Applied Mechanics
        and Engineering* 71.2 (1988), pp. 197 –224. ISSN: 0045-7825.

[22]   D. Kraft. *A Software Package for Sequential Quadratic Programming*. Deutsche Forschungs-
        und Versuchsanstalt für Luft- und Raumfahrt Köln: Forschungsbericht. Wiss. Berichtswe-
        sen d. DFVLR, 1988.

[23]   "Chapter 5 - Genetic Algorithms". In: *Pattern Recognition and Signal Analysis in
        Medical Imaging (Second Edition)*. Ed. by A. Meyer-Baese and V. Schmid. Second
        Edition. Oxford: Academic Press, 2014, pp. 135 –149.

[24]   O. Sigmund and K. Maute. "Topology optimization approaches". In: *Structural
        and Multidisciplinary Optimization* 48.6 (Dec. 2013), pp. 1031–1055.

[25]   S. Osher and J. A. Sethian. "Fronts propagating with curvature-dependent speed:
        Algorithms based on Hamilton-Jacobi formulations". In: *Journal of Computational
        Physics* 79.1 (1988), pp. 12 –49. ISSN: 0021-9991.

[26]   S. K. Godunov. "A difference method for numerical calculation of discontinu-
        ous solutions of the equations of hydrodynamics". In: *Matematicheskii Sbornik* 89.3
        (1959), pp. 271–306.

[27]   J. A. Sethian and A. Wiegmann. "Structural Boundary Design via Level Set and
        Immersed Interface Methods". In: *Journal of Computational Physics* 163.2 (2000),
        pp. 489 –528.

[28]   G. Allaire, F Jouve, and A. Toader. "A level-set method for shape optimization".
        In: *Comptes Rendus Mathematique* 334.12 (2002), pp. 1125 –1130.

[29]   G. Allaire, F. Jouve, and A. Toader. "Structural optimization using sensitivity
        analysis and a level-set method". In: *Journal of Computational Physics* 194.1 (2004),
        pp. 363 –393.

[30]   M. Y. Wang, X. Wang, and D. Guo. "A level set method for structural topology
        optimization". In: *Computer Methods in Applied Mechanics and Engineering* 192.1
        (2003), pp. 227 –246. ISSN: 0045-7825.

[31]   G. Allaire and F. Jouve. "Minimum stress optimal design with the level set method". In: *Engineering Analysis with Boundary Elements* 32.11 (2008). Shape and Topological Sensitivity Analysis: Theory and Applications, pp. 909 –918. ISSN: 0955-7997.

[32]   K. Suresh and M. Takalloozadeh. "Stress-constrained topology optimization: a topological level-set approach". In: *Structural and Multidisciplinary Optimization* 48.2 (Aug. 2013), pp. 295–309.

[33]   Q. Xia et al. "A level set solution to the stress-based structural shape and topology optimization". In: *Computers & Structures* 90-91 (2012), pp. 55–64. ISSN: 0045-7949.

[34]   P. Wei et al. "An 88-line MATLAB code for the parameterized level set method based topology optimization using radial basis functions". In: *Structural and Multidisciplinary Optimization* 58.2 (Aug. 2018), pp. 831–849. ISSN: 1615-1488.

[35]   G. I. N. Rozvany. "A critical review of established methods of structural topology optimization". In: *Structural and Multidisciplinary Optimization* 37.3 (Jan. 2009), pp. 217–237. ISSN: 1615-1488.

[36]   M. P. Bendsøe. "Optimal shape design as a material distribution problem". In: *Structural optimization* 1.4 (Dec. 1989), pp. 193–202.

[37]   M. P. Bendsøe and O. Sigmund. *Optimization of structural topology, shape, and material*. Vol. 414. Springer, 1995.

[38]   E. Tyflopoulos et al. "State of the art of generative design and topology optimization and potential research needs". In: *DS 91: Proceedings of NordDesign 2018, Linköping, Sweden, 14th-17th August 2018 DESIGN IN THE ERA OF DIGITALIZATION* (2018).

[39]   N. F. Wang and X. M. Zhang. "A Solid Isotropic Material with Parallel Penalization method for structural topology optimization with multiple materials". In: *2016 International Conference on Manipulation, Automation and Robotics at Small Scales (MARSS)*. July 2016, pp. 1–6.

[40]   M. Stolpe and K. Svanberg. "On the trajectories of penalization methods for topology optimization". In: *Structural and Multidisciplinary Optimization* 21.2 (Apr. 2001), pp. 128–139.

[41]   G. Allaire and G. A. Francfort. "A Numerical Algorithm for Topology and Shape Optimization". In: *Topology Design of Structures*. Ed. by M. P Bendsøe and C. A. M. Soares. Dordrecht: Springer Netherlands, 1993, pp. 239–248.

[42]   G. Allaire and R. V. Kohn. "Topology Optimization and Optimal Shape Design Using Homogenization". In: *Topology Design of Structures*. Ed. by M. P. Bendsøe and C. A. M Soares. Dordrecht: Springer Netherlands, 1993, pp. 207–218.

[43]   O. Sigmund and J. Petersson. "Numerical instabilities in topology optimization: A survey on procedures dealing with checkerboards, mesh-dependencies and local minima". In: *Structural optimization* 16.1 (Aug. 1998), pp. 68–75.

[44]   M. Stolpe and K. Svanberg. "An alternative interpolation scheme for minimum compliance topology optimization". In: *Structural and Multidisciplinary Optimization* 22.2 (Sept. 2001), pp. 116–124.

[45]   Z. Luo et al. "Compliant mechanism design using multi-objective topology optimization scheme of continuum structures". In: *Structural and Multidisciplinary Optimization* 30.2 (Aug. 2005), pp. 142–154.

[46]   G. Allaire. "The Homogenization Method for Topology and Shape Optimization". In: *Topology Optimization in Structural Mechanics*. Ed. by G. I. N. Rozvany. Vienna: Springer Vienna, 1997, pp. 101–133.

[47]   M. Zhou and G. I. N. Rozvany. "On the validity of ESO type methods in topology optimization". In: *Structural and Multidisciplinary Optimization* 21.1 (Mar. 2001), pp. 80–83.

[48]   W. Dorn. "Automatic design of optimal structures". In: *J. de Mecanique* 3 (1964), pp. 25–52.

[49]   T. Hagishita and M. Ohsaki. "Topology optimization of trusses by growing ground structure method". In: *Structural and Multidisciplinary Optimization* 37.4 (Jan. 2009), pp. 377–393.

[50]   T. Zegard and G. H. Paulino. "GRAND — Ground structure based topology optimization for arbitrary 2D domains using MATLAB". In: *Structural and Multidisciplinary Optimization* 50.5 (Nov. 2014), pp. 861–882. ISSN: 1615-1488.

[51]   M. Alzahrani, S. Choi, and D. W. Rosen. "Design of truss-like cellular structures using relative density mapping method". In: *Materials & Design* 85 (2015), pp. 349–360. ISSN: 0264-1275.

[52]   P. Zhang et al. "Efficient Design-Optimization of Variable-Density Hexagonal Cellular Structure by Additive Manufacturing: Theory and Validation". In: *Journal of Manufacturing Science and Engineering* 137.2 (Apr. 2015), pp. 021004–021004–8. ISSN: 1087-1357.

[53]   J. Wu et al. "Self-supporting rhombic infill structures for additive manufacturing". In: *Computer-Aided Design* 80 (2016), pp. 32 –42. ISSN: 0010-4485.

[54]   J. C. Steuben, A. P. Iliopoulos, and J. G. Michopoulos. "Implicit slicing for functionally tailored additive manufacturing". In: *Computer-Aided Design* 77 (2016), pp. 107 –119. ISSN: 0010-4485.

[55]   J. Liu et al. "Light-weight shape and topology optimization with hybrid deposition path planning for FDM parts". In: *The International Journal of Advanced Manufacturing Technology* 97.1 (July 2018), pp. 1123–1135.

[56]   A. Bellini and S. Güçeri. "Mechanical characterization of parts fabricated using fused deposition modeling". In: *Rapid Prototyping Journal* 9.4 (2003), pp. 252–264.

[57]   P. Zhang, J. Liu, and A. C. To. "Role of anisotropic properties on topology optimization of additive manufactured load bearing structures". In: *Scripta Materialia* 135 (2017), pp. 148 –152. ISSN: 1359-6462.

[58]   C. Koch, L. V. Hulle, and N. Rudolph. "Investigation of mechanical anisotropy of the fused filament fabrication process via customized tool path generation". In: *Additive Manufacturing* 16 (2017), pp. 138 –145. ISSN: 2214-8604.

[59]   B. Wittbrodt and J. M. Pearce. "The effects of PLA color on material properties of 3-D printed components". In: *Additive Manufacturing* 8 (2015), pp. 110 –116. ISSN: 2214-8604.

[60]   K. M. Tam and C. T. Mueller. "Additive Manufacturing Along Principal Stress Lines". In: *3D Printing and Additive Manufacturing* 4.2 (2017), pp. 63–81.

[61]   E. Andreassen et al. "Efficient topology optimization in MATLAB using 88 lines of code". In: *Structural and Multidisciplinary Optimization* 43.1 (Jan. 2011), pp. 1–16.

[62]   A. G. M. Michell. "LVIII. The limits of economy of material in frame-structures". In: *The London, Edinburgh, and Dublin Philosophical Magazine and Journal of Science* 8.47 (1904), pp. 589–597.

[63]   Y. Li and Y. Chen. "Beam structure optimization for additive manufacturing based on principal stress lines". In: *Solid Freeform Fabrication Proceedings*. 2010, pp. 666–678.